State Space Analysis of Variable-Stiffness Tendon Drive with Non-back-Drivable Worm-Gear Motor Actuation

Howard, Ian S.; Stoelen, Martin F.

Published in:
Host publication not specified in Elements

DOI:
10.1007/978-3-030-89177-0_30

Publication date:
2021

State space analysis of variable-stiffness tendon drive with non-back-drivable worm-gear motor actuation

Ian S. Howard[1] & Martin F. Stoelen[2,3]

[1]SECAM, University of Plymouth, Plymouth, PL4 8AA UK.
[2]Western Norway University of Applied Science, Førde, Norway.
[3]Fieldwork Robotics Ltd, Cambridge, CB24 9AD UK
ian.howard@plymouth.ac.uk, Martin.Fodstad.Stolen@hvl.no

Abstract. Here we investigate variable-stiffness tendon drive for a robot arm. The novel aspect of our design is that it makes use of non-back-drivable worm-gear motor actuation, so static arm configurations can be maintained at a desired stiffness level without requiring motor power. We first analyze a link that is driven via uni-directional agonistic-antagonistic non-linear elastic tendons and construct the state space model of the system. We then design an observer-based state feedback controller. This ensures the output link can track a reference input vector consisting of a desired joint angle as well as tendon extension realized by tendon co-contraction. We simulated the controller and plant in MATLAB and show examples of typical movement trajectories for angular control of the link.

Keywords: Agonistic-antagonistic tendons, Worm drive, State space control.

1 Introduction

There is much interest in the development of actuators that exhibit compliance [1,2], and there are many potential applications areas for compliant robotic arms. They are well suited for operation in unstructured environments where occasional collisions are possible and are potentially safe around people. High compliance is not always desirable and variable compliance assists payloads manipulation [3], and high stiffness assists operation with unstable loads, as it does in human manipulation and movement [4]. Various methods have been proposed to implement compliance and modulate stiffness [2]. We extend the approach taken in the Gummiarm, which achieves variable stiffness by means of non-linear elastic tendon co-contraction [5]. We use a uni-directional agonist-antagonist tendon setup, but bi-directional designs are also possible [6]. Here we use low-cost worm-gear motor actuation, which is not back drivable, to ensure static joint configuration at a fixed tendon tension and consequently fixed joint stiffness, can be maintained without requiring drive to the motors. This makes the overall design power-efficient and well suited to mobile applications. An example could a mobile autonomous berry picking system, where compliance increases robustness to collisions and power consumption must be minimized to extend operating time between recharging of the platform's batteries.

2 Tendon drive system

Much previous work has been done on tendon driven mechanisms [7]. Here we analyse the motor-tendon system illustrated in Fig.1A and develop a state space description. A feedback controller is used to drive the motors that operate the left and right pulleys, ensuring the output angle follows the reference input angle. Similarly, the controller maintains co-contraction to achieve a target tendon extension. Turning both input pulleys in opposite directions increases tension in both tendons, but results in no net torque on the output pulley and it remains stationary. Rotating them in the same direction results in a net torque, which causes the output pulley to rotate. A rod representing a robot link is attached to the output pulley, as shown in Fig. 1B. This resists the applied torque due to viscous friction from the bearing and air, and due to the moment of inertia of the rotating components. Brushed worm-drive DC motors rotate the pulleys.

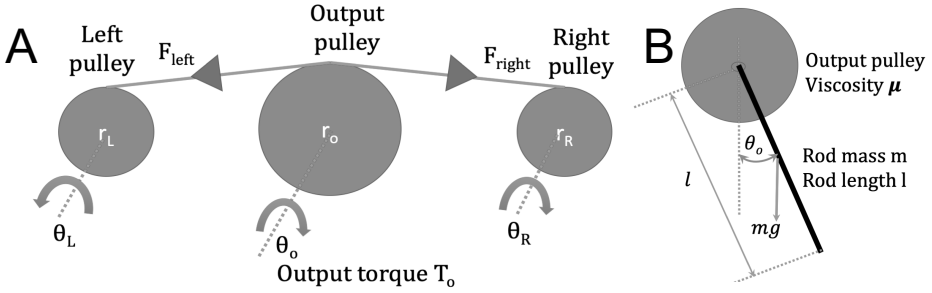

Fig 1. Panel A: Schematic of agonist-antagonist two-tendon drive. The tendons wrap-around and are firmly attached to the pulleys and do not just rely of friction to transfer force. Panel B: Simple robot link connected to the output pulley.

3 State space analysis of DC motor

Many researchers have investigated the analysis and control of DC motors, e.g. [8,9], including those that make the use of worm gear drives [10,11]. Here we run DC motors under voltage control. Consider the equivalent circuit of a single DC motor as shown in Fig. 2. Motor torque T_m generated by current passing through the motor coils is given by the product of armature current and the motor torque constant k_t.

$$T_m = k_t i \tag{1}$$

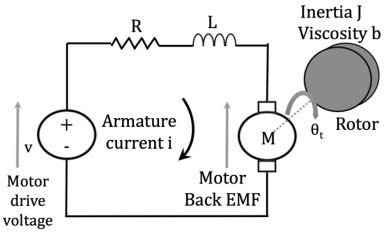

Fig 2. Equivalent electrical circuit of a DC motor, including armature mechanical properties.

Motor torque T_m is resisted by the motor's inertia J, as well as its viscous friction b

$$T_m = b\frac{d\theta_t}{dt} + J\frac{d^2\theta_t}{dt^2} \tag{2}$$

Equating the two terms gives

$$k_t i = b\frac{d\theta_t}{dt} + J\frac{d^2\theta_t}{dt^2} \tag{3}$$

$$\Rightarrow \frac{d}{dt}(\dot{\theta}_t) = -\frac{b}{J}\dot{\theta}_t + \frac{k_t}{J}i \tag{4}$$

Summing voltages around the circuit leads to a voltage equation, where v represents the motor control input voltage, L is motor inductance, R motor resistance, and K_e is motor generator constant

$$v = iR + L\frac{di}{dt} + k_e\frac{d\theta_t}{dt} \tag{5}$$

$$\Rightarrow \frac{d}{dt}(i) = -\frac{k_e}{L}\dot{\theta}_t - \frac{R}{L}i + \frac{1}{L}v \tag{6}$$

Choosing the states and the input as the voltage applied to the motor

$$x_1 = \dot{\theta}_t \tag{7}$$

$$x_2 = i \tag{8}$$

$$\Rightarrow \frac{d}{dt}(x_1) = -\frac{b}{J}x_1 + \frac{k_t}{J}x_2 \tag{9}$$

$$\Rightarrow \frac{d}{dt}(x_2) = -\frac{k_e}{L}x_1 - \frac{R}{L}x_2 + \frac{1}{L}v \tag{10}$$

Angular position output can be computed by integrating motor angular velocity, so

$$\frac{d}{dt}(x_3) = x_1 \tag{11}$$

This leads to the state space matrix equation for a motor

$$\Rightarrow \frac{d}{dt}\begin{bmatrix} x_1 \\ x_2 \\ x_3 \end{bmatrix} = \begin{bmatrix} -\frac{b}{J} & \frac{k_t}{J} & 0 \\ -\frac{k_e}{L} & -\frac{R}{L} & 0 \\ 1 & 0 & 0 \end{bmatrix}\begin{bmatrix} x_1 \\ x_2 \\ x_3 \end{bmatrix} + \begin{bmatrix} 0 \\ \frac{1}{L} \\ 0 \end{bmatrix}v \tag{12}$$

We represent the worm gear motor gearing ratio by G_e which increases the mechanical advantage and scales the overall motor output position by a factor $\frac{1}{G_e}$. We note in practice that $K_t = K_e$ but choose to keep them separate here for clarity.

4 Analysis of Two-Tendon Rotary Series Elastic Actuator

4.1 Modeling tendon extension

In an agonistic-antagonist arrangement, if tendon extension force is a quadratic function of extension, then stiffness is a linearly function of extension [12,13]. However, for small displacement around their extension point, we can consider the tendons as locally linear springs with spring constant k, so local force is proportional to local extension. Thus, the local linear constant k is dependent on tension, which can be modulated by co-contraction. We assume that both tendon springs are always operating under pre-tension, so neither ever goes slack. With drive and output angles in radians, output torque is given by the differences in torques exerted by the right and left tendons

$$T_o = k(\theta_R r_R - \theta_o r_o) r_o - k(\theta_o r_o + \theta_L r_L) r_o \tag{13}$$

Where +ve directions are shown on Fig, 1. If both drive pulleys have same radius r_{in}

$$T_o = k r_o((\theta_R - \theta_L) r_{in} - 2\theta_o r_o) \tag{14}$$

We can re-write the expression in terms of a new spring constant $K_r = k r_o^2$

$$T_o = K_r \left(\frac{r_{in}}{r_o}(\theta_R - \theta_L) - 2\theta_o\right) \tag{15}$$

4.2 Modeling to 2-tendon actuator dynamics

When the link (modelled as a rod) moves in a vertical plane, the torque exerted on the output pulley by the tendons is resisted by mechanism's inertia I, a torque term arising from the gravity and viscous friction μ.

$$T_o = I\ddot{\theta}_o + \mu\dot{\theta}_o + \frac{mgl}{2}\sin(\theta_o) \tag{16}$$

Equating the two expressions

$$K_r \left(\frac{r_{in}}{r_o}(\theta_R - \theta_L) - 2\theta_o\right) = I\ddot{\theta}_o + \mu\dot{\theta}_o + \frac{mgl}{2}\sin(\theta_o) \tag{17}$$

Rearranging with only the highest order differential on the LHS

$$\ddot{\theta}_o = -\frac{\mu}{I}\dot{\theta}_o - \frac{mgl}{2I}\sin(\theta_o) - \frac{2K_r}{I}\theta_o + \frac{K_r}{I}\frac{r_{in}}{r_o}(\theta_R - \theta_L) \tag{18}$$

We note the gravity term will be small in comparison to the restoring force due to tendon stiffness. It is also zero when the link moves horizontally. More generally, when the link is hanging down vertically, linearizing for small angles gives

$$\ddot{\theta}_o = -\frac{\mu}{I}\dot{\theta}_o - \left(\frac{mgl}{2I} + \frac{2K_r}{I}\right)\theta_o + \frac{K_r}{I}\frac{r_{in}}{r_o}(\theta_R - \theta_L) \tag{19}$$

4.3 State space model of 2-tendon drive dynamics

To build a state space model of this 2-tendon system we choose states x_1 and x_2

$$x_1 = \dot{\theta_o} \tag{20}$$

$$x_2 = \theta_o \Rightarrow \dot{x_2} = \dot{\theta_o} = x_1 \tag{21}$$

This leads to two 1st order equations

$$\dot{x_1} = -\frac{\mu}{I}x_1 - \left(\frac{mgl}{2I} + \frac{2K_r}{I}\right)x_2 + \frac{K_r}{I}\frac{r_{in}}{r_o}\theta_R - \frac{K_r}{I}\frac{r_{in}}{r_o}\theta_L \tag{22}$$

$$\dot{x_2} = \dot{\theta_o} = x_1 \tag{23}$$

Writing in matrix form gives the state space equations

$$\Rightarrow \frac{d}{dt}\begin{bmatrix} x_1 \\ x_2 \end{bmatrix} = \begin{bmatrix} -\frac{\mu}{I} & -\left(\frac{mgl}{2I} + \frac{2K_r}{I}\right) \\ 1 & 0 \end{bmatrix}\begin{bmatrix} x_1 \\ x_2 \end{bmatrix} + \begin{bmatrix} \frac{K_r}{I}\frac{r_{in}}{r_o} & -\frac{K_r}{I}\frac{r_{in}}{r_o} \\ 0 & 0 \end{bmatrix}\begin{bmatrix} \theta_R \\ \theta_L \end{bmatrix} \tag{24}$$

4.4 Tendon extension and output actuation

When the link is in equilibrium position hanging downwards or is horizontal, and exerting no load on the tendons, tension stretching is only due to the co-contraction extension from the control pulleys (again note rotation directions on Fig. 1)

$$\theta_{\boldsymbol{stretch}} = (\theta_{\boldsymbol{R}} + \theta_{\boldsymbol{L}}) \tag{25}$$

$$\Rightarrow \theta_R = \theta_{stretch} - \theta_L \tag{26}$$

$$\Rightarrow \theta_L = \theta_{stretch} - \theta_R \tag{27}$$

Output angle will be midway between the two control angles

$$\theta_{\boldsymbol{target}} = \frac{(\theta_{\boldsymbol{R}} - \theta_{\boldsymbol{L}})}{2} \tag{28}$$

Substituting for θ_R from equation (26)

$$\Rightarrow \theta_{target} = \frac{(\theta_{stretch} - \theta_L - \theta_L)}{2} \tag{29}$$

$$\Rightarrow \theta_L = \frac{\theta_{stretch}}{2} - \theta_{target} \tag{30}$$

Substituting for θ_L from equation (27)

$$\Rightarrow \theta_{target} = \frac{(\theta_R - \theta_{stretch} + \theta_R)}{2} \tag{31}$$

$$\Rightarrow \theta_R = \theta_{target} + \frac{\theta_{stretch}}{2} \tag{32}$$

5 State space model for motor driven 2-tendon drive

We now build as single state space model for two DC worm-drive motors and the tendon dynamics for the unloaded arm. Since we use a worm drive gear that is not back-drivable and the load on the motors due to arm is very low, we assume the output position of the worm gear motors are unaffected by the link mechanism. However, we could easily add an additional effective inertial term to the motor to account for the link's inertial resistance. Given our simplifying assumptions, the tendons are only influenced by motor output actuator angles. We can thus combine the state space models for motor actuation and tendon drive into single matrix as follows:

$$\frac{d}{dt}\begin{bmatrix} x_1 \\ x_2 \\ x_3 \\ x_4 \\ x_5 \\ x_6 \\ x_7 \\ x_8 \end{bmatrix} = A\begin{bmatrix} x_1 \\ x_2 \\ x_3 \\ x_4 \\ x_5 \\ x_6 \\ x_7 \\ x_8 \end{bmatrix} + B\begin{bmatrix} \theta_{target} \\ \theta_{stretch} \end{bmatrix} \tag{33}$$

Where the A and B matrices are given by equations (34) and (35). It can be seen that the 3x3 regions in the A matrix denoted by the black rectangles represent the state space matrix contributions from the two motors and follow the A matrix in equation (12). We drive these two motors with target angle and co-contraction stretch extension inputs in the input vector $[\theta_{target} \quad \theta_{stretch}]^T$, where θ_{target} is the joint output target angle and $\theta_{stretch}$is co-contraction. These inputs are mapped onto the control inputs for the left and right motors by equations (30) and (32), as implemented in the combined input matrix B given in (35); note the transpose. A full list of parameters is given in Table 1.

$$A = \begin{bmatrix} -\frac{b}{J} & \frac{Kt}{J} & 0 & 0 & 0 & 0 & 0 & 0 \\ -\frac{Ke}{L} & -\frac{R}{L} & 0 & 0 & 0 & 0 & 0 & 0 \\ 1 & 0 & 0 & 0 & 0 & 0 & 0 & 0 \\ 0 & 0 & 0 & -\frac{b}{J} & \frac{Kt}{J} & 0 & 0 & 0 \\ 0 & 0 & 0 & -\frac{Ke}{L} & -\frac{R}{L} & 0 & 0 & 0 \\ 0 & 0 & 0 & 1 & 0 & 0 & 0 & 0 \\ 0 & 0 & \frac{Kr}{\mathrm{G_e} I}\frac{\mathrm{r_{in}}}{\mathrm{r_o}} & 0 & 0 & -\frac{Kr}{\mathrm{G_e} I}\frac{\mathrm{r_{in}}}{\mathrm{r_o}} & -\frac{\mu}{I} & -\left(\frac{mgl}{2I}+\frac{2Kr}{I}\right) \\ 0 & 0 & 0 & 0 & 0 & 0 & 1 & 0 \end{bmatrix} \tag{34}$$

$$B = \begin{bmatrix} 0 & -\frac{1}{L} & 0 & 0 & \frac{1}{L} & 0 & 0 & 0 \\ 0 & \frac{1}{2L} & 0 & 0 & \frac{1}{2L} & 0 & 0 & 0 \end{bmatrix}^T \tag{35}$$

The states x_3 and x_6 represent motor drive angles prior to reduction by the worm gears. These values are scaled by the reciprocal of the gearing ratio and drive the input to the left and right tendon pulley system. The latter is represented by the lower dashed rectangle, which follows the A matrix for the tendon dynamics captured in equation (24). This leads to a system with 8 states in total. To implement state feedback control we need to estimate the full system state. We use a Luenberger observer for this purpose. Fig 3. shows the structure of the controller. Since motor and link angular velocities are be hard to measure directly in a mechanical implementation, they are estimated. However angular position from the motors, motor currents, and output link angle are often available and can be used to correct the state estimate. The C matrix shown in equation (36) thus selects motor current, position and link position from the full state vector:

Table 1. List of all parameters for agonist-antagonist compliant drive system

	Link and tendon			**Worm-drive motor**
I	Link mechanism's inertia		L	Motor inductance
mg	Link gravity force term		R	Motor resistance
μ	Link viscous friction coefficient		J	Motor inertia
K_r	Effective tendon spring constant		b	Motor viscous friction
r_{in}	Drive pulley radius		G_e	Worm gearing ratio
r_o	Output pulley radius		K_e	Motor generator constant
l	Link length		K_t	Motor torque constant

6 Observer-based state feedback control of link angle

To find a linear quadratic regulator gain K to implement full state feedback control of the system, diagonal terms in the Q and R matrices were specified, to penalized the system states and controls.

$$\begin{bmatrix} y_1 \\ y_2 \\ y_3 \\ y_4 \\ y_5 \end{bmatrix} = \begin{bmatrix} 0 & 1 & 0 & 0 & 0 & 0 & 0 & 0 \\ 0 & 0 & 1 & 0 & 0 & 0 & 0 & 0 \\ 0 & 0 & 0 & 0 & 1 & 0 & 0 & 0 \\ 0 & 0 & 0 & 0 & 0 & 1 & 0 & 0 \\ 0 & 0 & 0 & 0 & 0 & 0 & 0 & 1 \end{bmatrix} \begin{bmatrix} x_1 \\ x_2 \\ x_3 \\ x_4 \\ x_5 \\ x_6 \\ x_7 \\ x_8 \end{bmatrix} \tag{36}$$

They consisted of costs for the motor states $Cost_{mv} = 0.01$, $Cost_{ml} = 0.01$ and $Cost_{ma} = 10$ for the motor velocity, current and angle respectively. In addition, costs were specified for the tendon system consisting of $Cost_{lv} = 0.01$ and $Cost_{la} = 10$ for the link velocity and angle states. The values used were found by experimentation. The cost matrix Q was composed of these elements:

$$Q = \begin{bmatrix} Cost_{\mathrm{mv}} & 0 & 0 & 0 & 0 & 0 & 0 & 0 \\ 0 & Cost_{\mathrm{mi}} & 0 & 0 & 0 & 0 & 0 & 0 \\ 0 & 0 & Cost_{\mathrm{ma}} & 0 & 0 & 0 & 0 & 0 \\ 0 & 0 & 0 & Cost_{\mathrm{mv}} & 0 & 0 & 0 & 0 \\ 0 & 0 & 0 & 0 & Cost_{\mathrm{mi}} & 0 & 0 & 0 \\ 0 & 0 & 0 & 0 & 0 & Cost_{\mathrm{ma}} & 0 & 0 \\ 0 & 0 & 0 & 0 & 0 & 0 & Cost_{\mathrm{lv}} & 0 \\ 0 & 0 & 0 & 0 & 0 & 0 & 0 & Cost_{la} \end{bmatrix} \quad (37)$$

Similarly, the control voltages to the motors were penalized by $\mathrm{Cost_{cv}}$ terms along the diagonal of the R matrix:

$$\mathrm{R} = \begin{bmatrix} Cost_{\mathrm{cv}} & 0 \\ 0 & Cost_{\mathrm{cv}} \end{bmatrix} \quad (38)$$

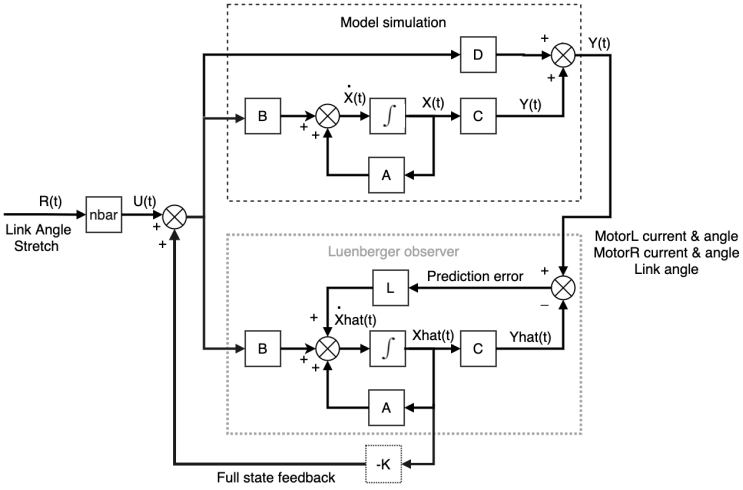

Fig. 3. Signal flow graph of tendon drive model under observer-based state feedback control.

For weak control penalization we set $Cost_{\mathrm{cv}}$ = 5 and for strong control penalization $Cost_{\mathrm{cv}}$ = 50. Pre-compensation was implemented to track the reference link angle target by computing nbar, so that the corresponding angular position DC gain of the system was unity. The Luenberger observer state estimator uses the state space a model of the plant as captured by the matrices A and B, given in equations (34,35), and a correction term arising from the difference between actual and predicted output. The Luenberger gain L was again calculated using the MATLAB lqr command. The state space controller was implemented in MATLAB and the trapezoid method was used to implement integration, which is also suitable for a real-time implementation [14].

7 Results and conclusions

Simulation results are shown in Fig 4. Panels A-C show results when low control voltage penalization of 5 was used and no limits were placed on the drive voltage to the

motors. We use a point to point angular movement task, which is representative of typical operation. The target joint angle follows a sequence of 2-second-long values held at [0 ,1 ,0, -1, 0] Rad. It can be seen that the link follows the target angle specified with a rise time of about 200ms. To demonstrate that extending the tendons due to co-contraction does not affect output angle, the extension angle simultaneous follows the sequence of [0, 0.5, 0, -0,5, 0]. Panels B and C show the link velocity and motor voltages rises to high values. Panels D-E show results when control voltage penalization of 50 was used, with limits placed on the motors of 48v (to simulate the effects of using a real controller with the motors). Results in panel D shows that more cost for the voltage drive to the motors and clipping the maximum values slows down the rise time to about 700ms, although this system still reaches the target link angle. The limitation on motor voltages makes the latter scenario suitable for a real-time hardware implementation.

To summarize, we analysed a variable-stiffness tendon drive system using worm gear actuation. The non-back drivability of the drive lead to a simplifying assumption that the tendon mechanism was uncoupled from the dynamics of the motor and vice-versa. Simulation showed observer-based state feedback control can realise angle position control of a single link. Results from an EtherCAT implementation on a mechanical motor-driven tendon system are described in a companion manuscript [14].

8 Acknowledgments

We thank Simon Bates and Innovate UK project No: 104622 SoSehRaH, and the University of Plymouth for support, and Fieldwork Robotics Ltd for helpful discussion and access to their technology.

References

1. Grioli, G., Wolf, S., Garabini, M., Catalano, M., Burdet, E., Caldwell, D., & Bicchi, A. (2015). Variable stiffness actuators: The user's point of view. The International Journal of Robotics Research, 34(6), 727-743.
2. Vanderborght, B., Albu-Schäffer, A., Bicchi, A., Burdet, E., Caldwell, D.G., Carloni, R., Catalano, M.G., Eiberger, O., Friedl, W., Ganesh, G. and Garabini, M., (2013). Variable impedance actuators: A review. Robotics and autonomous systems, 61(12), pp.1601-1614. and Control (ICAC3) (pp. 1-5). IEEE.
3. Bicchi, A., & Tonietti, G. (2004). Fast and "soft-arm" tactics [robot arm design]. IEEE Robotics & Automation Magazine, 11(2), 22-33.
4. Burdet, E., Osu, R., Franklin, D.W., Milner, T.E. and Kawato, M., (2001). The central nervous system stabilizes unstable dynamics by learning optimal impedance. Nature, 414(6862), pp.446-449.
5. Stoelen, M.F., Bonsignorio, F. and Cangelosi, A., (2016), August. Co-exploring actuator antagonism and bio-inspired control in a printable robot arm. In International Conference on Simulation of Adaptive Behavior (pp. 244-255). Springer, Cham.
6. Petit, F., Friedl, W., Höppner, H. and Grebenstein, M., (2015). Analysis and synthesis of the bidirectional antagonistic variable stiffness mechanism, IEEE/ASME Transactions on Mechatronics, 20(2), pp.684-695.

7. Ozawa, R., Kobayashi, H., & Hashirii, K., (2013). Analysis, classification, and design of tendon-driven mechanisms. IEEE transactions on robotics, 30(2), 396-410.
8. Chotai, J., & Narwekar, K. (2017). Modelling and position control of brushed DC motor. In 2017 International Conference on Advances in Computing, Communication
9. Ruderman, M., Krettek, J., Hoffmann, F., & Bertram, T. (2008). Optimal state space control of DC motor. IFAC Proceedings Volumes, 41(2), 5796-5801.
10. Pinto, V. H., Gonçalves, J., & Costa, P. (2020). Model of a DC motor with worm gearbox. In Portuguese Conference on Automatic Control (pp. 638-647). Springer, Cham.
11. May, D. C., Jayasuriya, S., & Mooring, B. W. (2000). Modeling and control of a manipulator joint driven through a worm gear transmission. Journal of Vibration and Control, 6(1), 85-111.
12. Ham, R. V., Sugar, T., Vanderborght, B., Hollander, K., & Lefeber, D. (2009). Compliant actuator designs. IEEE Robotics & Automation Magazine, 3(16), 81-94.
13. Migliore, S. A., Brown, E. A., & DeWeerth, S. P. (2005). Biologically inspired joint stiffness control. In Proceedings of the 2005 IEEE international conference on robotics and automation (pp. 4508-4513). IEEE.
14. Howard I.S., Stoelen, M.F., (2021), EtherCAT implementation of a variable-stiffness tendon drive with non-back-drivable worm-gear motor actuation, TAROS 2021, University of Lincoln.

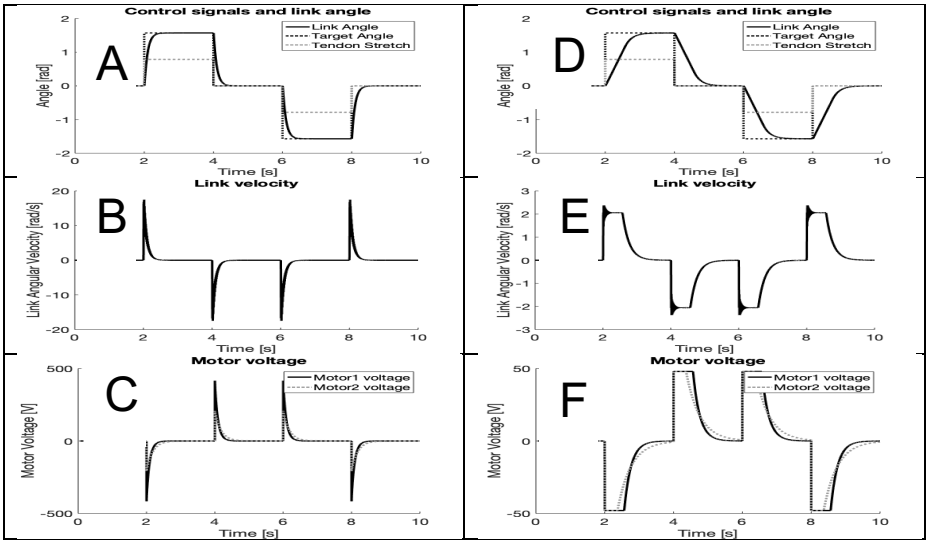

Fig 4. Simulation in MATLAB. Panels A-C for case when no limit was placed on the voltage control and its cost was small. Panels A The square wave envelope (black line) shows a positive and negative rectangular target angle applied to the controller. The response (solid line that quickly reaches the target) shows the link output link angle. Note that co-contraction results in tendon extension (dotted line) but had no effect on the output angle. Panel B shows the corresponding link velocity. Panel C shows the two motor control voltages. Panels D-E show the corresponding results when motor voltage magnitude is limited to 48v and voltage control cost was set a factor 5 higher than before. It can be seen penalized and limiting the drive voltage, necessary in a hardware implementation, affects behavior, but not catastrophically.